**Supplementary Information**

# ATPase-dependent role of the atypical kinase Rio2 on the evolving pre-40S subunit

Sébastien Ferreira-Cerca, Vatsala Sagar, Thorsten Schäfer, Momar Diop, Anne-Maria Wesseling, Haiyun Lu, Eileen Chai, Ed Hurt and Nicole LaRonde-LeBlanc

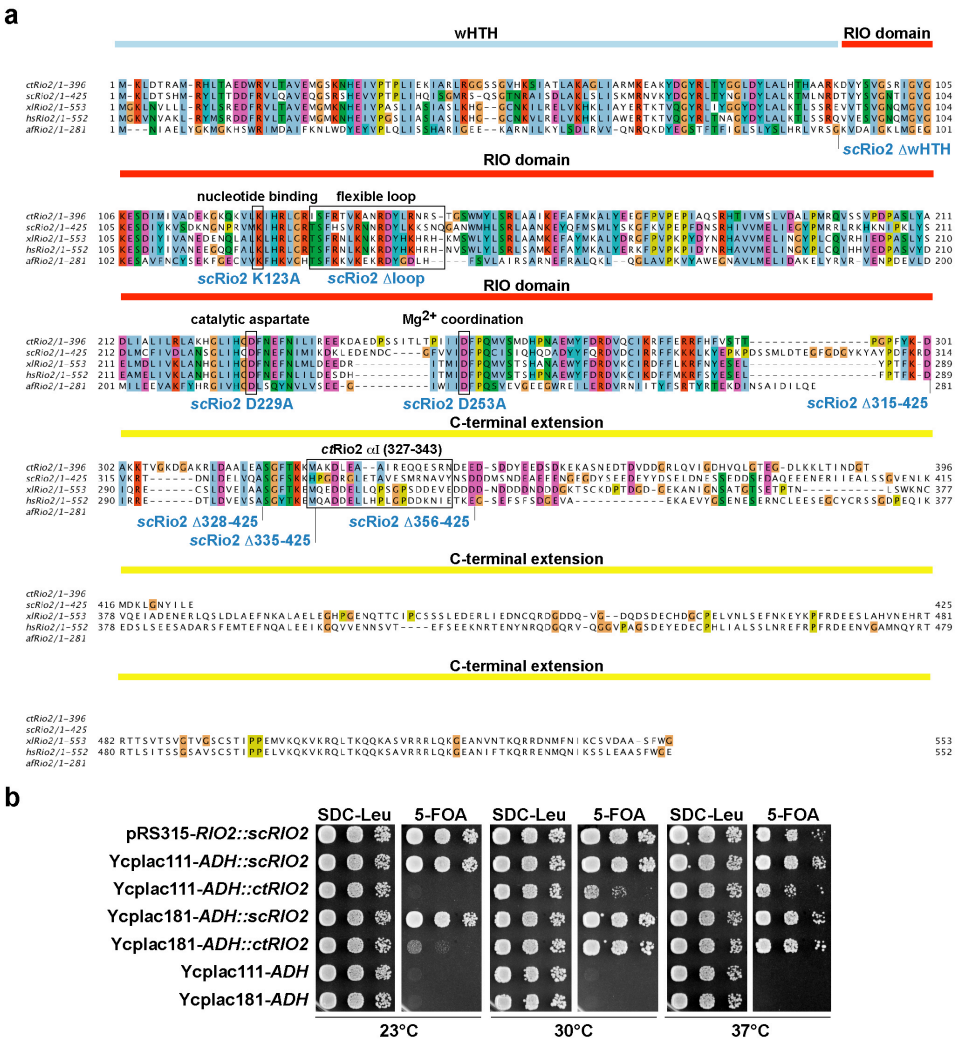


**Supplementary Figure 1 | The conserved *Chaetomium thermophilum* *ct*Rio2 can complement a yeast *rio2Δ* mutant. (a)** Multiple sequence alignment of eukaryotic Rio2 orthologs in comparison to archaeal Rio2. Sequence alignment of eukaryotic *ct*Rio2 (*Chaetomium thermophilum;* accession number CTHT_0033330), *sc*Rio2 (*Saccharomyces cerevisiae)*, *xl*Rio2 (*Xenopus laevis*), *hs*Rio2 (*Homo sapiens*) in comparison to archaeal *af*Rio2 (*Archaeoglobus fulgidus*) using T-Coffee multiple sequence alignment (http://www.ebi.ac.uk/Tools/msa/tcoffee) and Jalview. Indicated above the alignment are the different Rio2 structural domains including wHTH, RIO domain and C-terminal extension. Moreover, the kinase catalytic residues, the flexible loop and yeast Rio2 kinase point and deletion mutations (in blue) are indicated. **(b)** *ct*Rio2 can complement the yeast *rio2Δ* (null) mutant. Serial dilutions of the yeast *RIO2* shuffle strain (see Supplementary Table 2) transformed either with empty plasmid (Ycplac181-ADH), *scRIO2* and *ctRIO2* under the control of the constitutive *ADH* promoter in single or high copy number (2μ) plasmids (see Supplementary Table 3) were spotted on SDC-Leu (loading control) and SDC plates containing 5-FOA at the indicated temperature for 3 days.

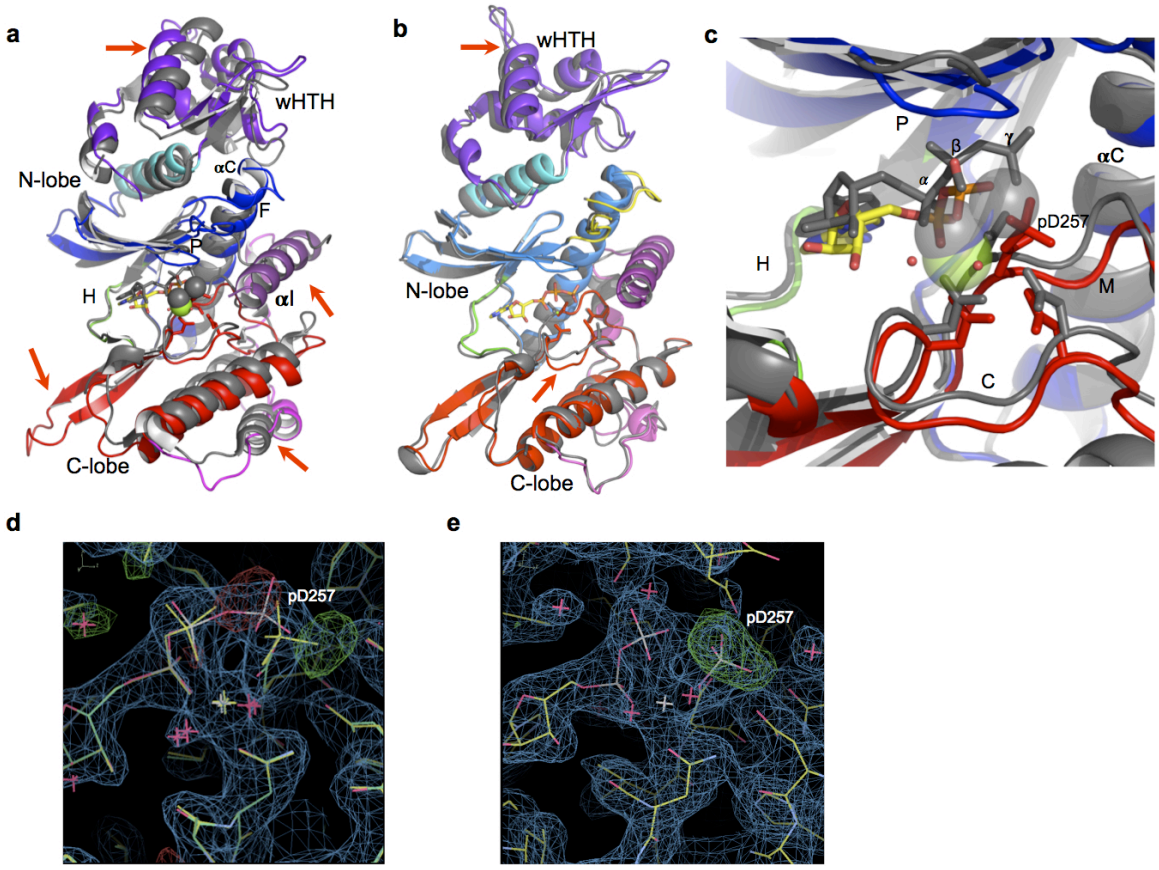


**Supplementary Figure 2 | Structure of the *ct*Rio2 kinase. (a)** Comparison of the overall structure of the *ct*Rio2 and *af*Rio2 kinases. *ct*Rio2 is colored according to subdomain while *af*Rio2 is shown in grey. Loops are labeled with **M**, **F**, **H**, **C** and **P** for metal-binding, flexible, hinge, catalytic and phosphate-binding loops respectively. Structural differences are indicated by arrows. **(b)** Comparison of the structure of *ct*Rio2::ATP complex with the APO structure. Very slight differences in relative positioning of the two domains and the active site loops are observed, indicated by arrows. **(c)** Close-up of *ct*Rio2 active site showing differences in positioning of metal ions and phosphates in *af*Rio2. **(d)** Electron density map calculated with ATP modeled in the *ct*Rio2 active site. Density in blue is 2Fo-Fc contoured at 1$\sigma$, and in red and green is Fo-Fc negative and positive difference density, respectively, contoured at 3$\sigma$. The yellow stick model is the model as is currently, after fitting a phosphoaspartate in place of the ATP $\gamma$-phosphate. **(e)** Fo-Fc difference density calculated after deletion of the phosphate group on top of the final model. Density is shown as in **d**.

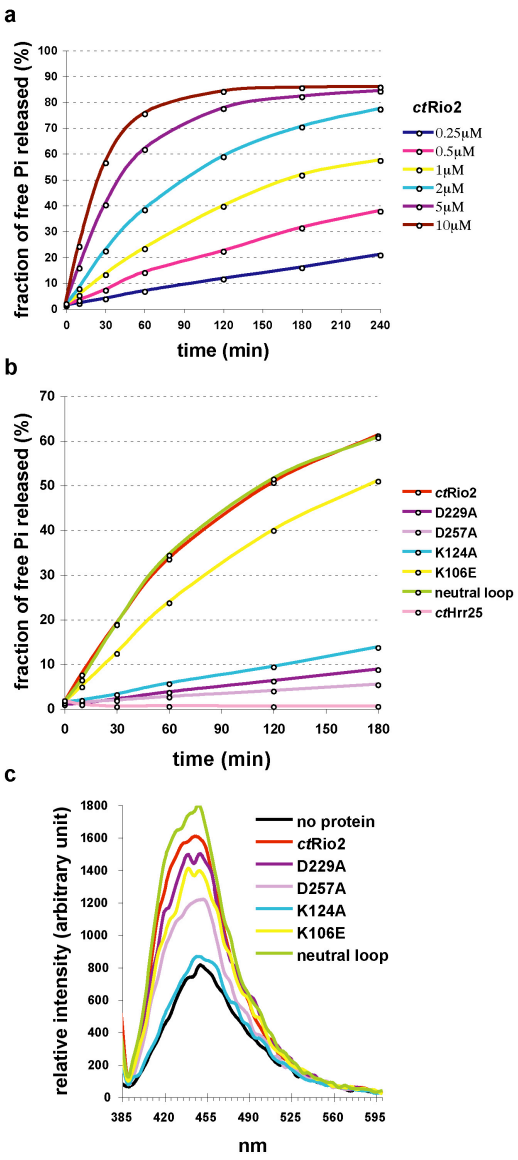


**Supplementary Figure 3 | *ct*Rio2 ATPase activity and nucleotide binding. (a, b)** the amount of released free phosphate ($P_i$) was analyzed in single-turnover experiments in presence of the indicated amount of purified recombinant protein and 50 nM ATP/ $\gamma^{32}$P-labeled ATP (see Online Methods). Reactions were stopped at the indicated time points. ATP and $P_i$ were separated by thin-layer chromatography and quantified with ImageJ. **(a)** *ct*Rio2 protein concentration-dependent $P_i$ release (ATPase activity) was performed with the indicated amount of purified *ct*Rio2 **(b)** analysis of free $P_i$ released in the presence of 1 μM purified *ct*Rio2 wild-type and mutants. **(c)** nucleotide binding was examined by measuring the change of fluorescence intensity (in arbitrary units) of mant-ATP ($\lambda_{ex}$ - 355 nm, $\lambda_{emax}$ - 440 nm) upon protein binding (see Supplementary Note). The intrinsic fluorescence by mant-ATP (no protein-black curve) is enhanced after the addition of *ct*Rio2 (red curve).

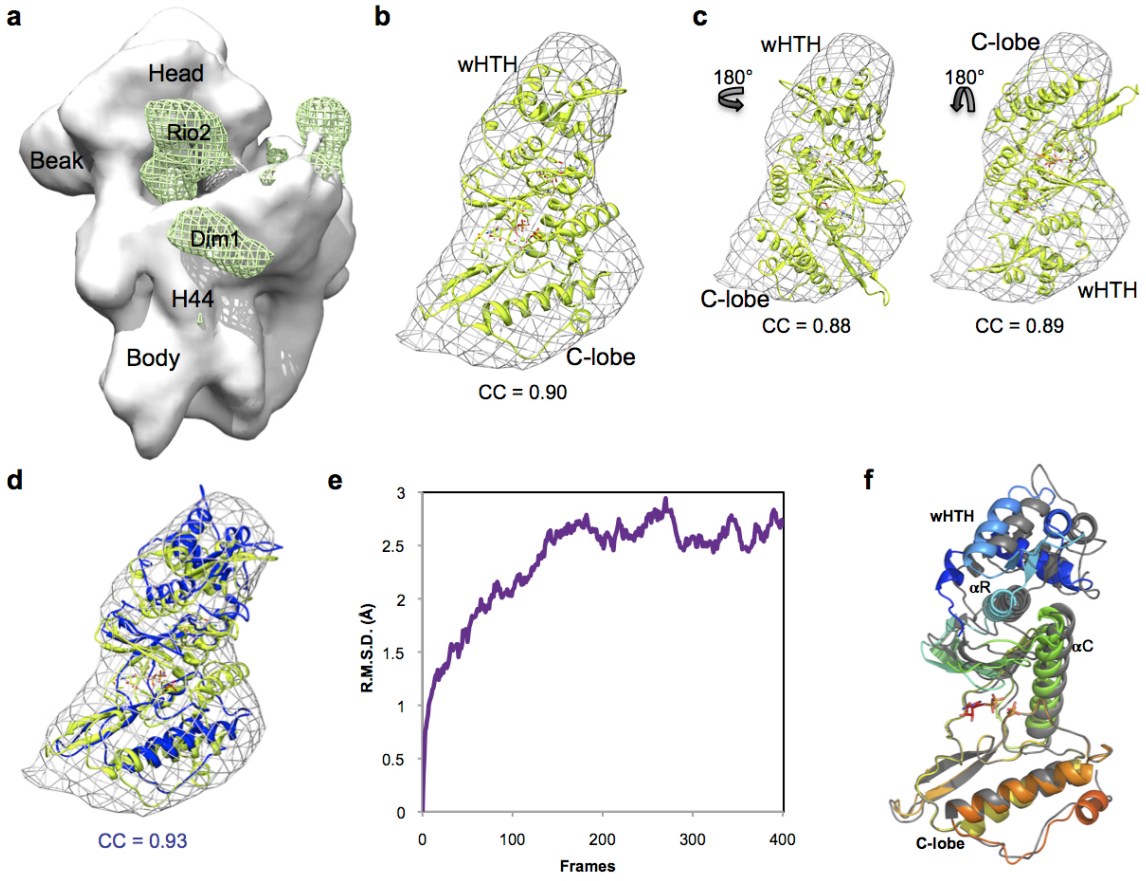


**Supplementary Figure 4 | Fitting of the eukaryotic Rio2 into cryo-EM density from yeast pre-40S particles. (a)** Difference density (green mesh) resulting from subtraction of cryo-EM density of the TAP-tagged Rio2-containing and Rio2-depleted pre-40S particles (grey solid). The main domains of the ribosome are labeled and assignment of difference density is identified as in Strunk et al[1,2]. **(b)** Best rigid body fit of *ct*Rio2 in the Rio2 difference density. Domains are labeled to provide orientation. **(c)** Fit of the molecule in two different orientations, rotated 180° around the vertical and horizontal axes. Both resulted in slightly lower correlation coefficients (CC; calculated in Chimera[1]). **(d)** Overlay of Molecular Dynamic Flexible Fit (MDFF)[3] model (blue) on starting model (yellow; same as in a). **(e)** Plot of RMSD's for all molecules in the MDFF trajectory relative to the starting model shows convergence after ~200 frames (200 ps). **(f)** Alignment of the C-terminal lobes of the *ct*Rio2::ATP complex (colored according to domains) and that of the MDFF model (grey) shows significant shift of the N-terminal lobe and the wHTH domains. The distance between the catalytic (C) and the phosphate-binding (P) loops increases by 1.6 Å, and there is a ~ 5.6 Å shift of the wHTH domain (measured by the change in distance between equivalent atoms in helices 2 and 3 of the domain).

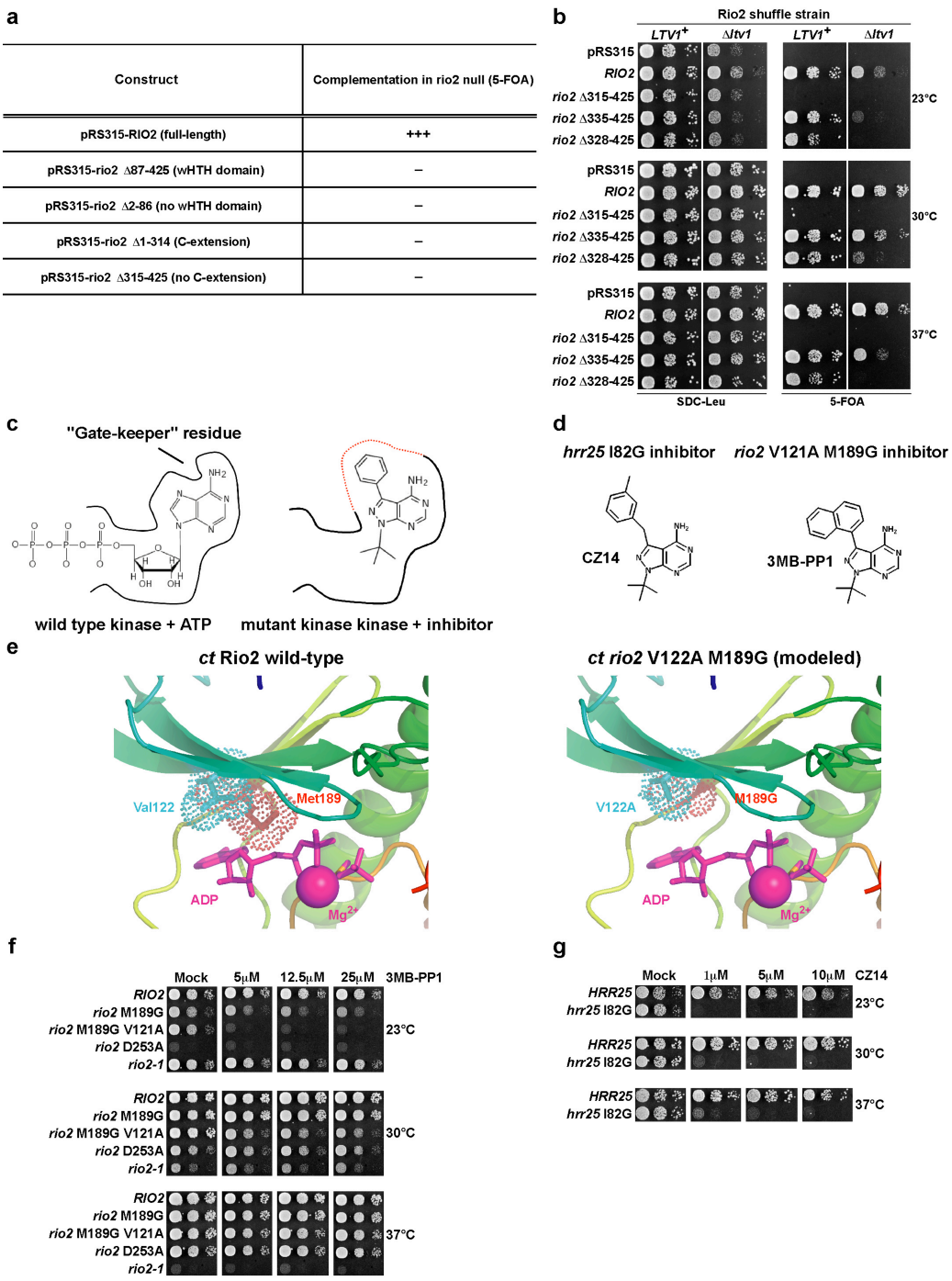


**Supplementary Figure 5 | Rio2 functional domain organization and generation of Hrr25 and Rio2 ATP-analogue sensitive strains. (a)** *sc*Rio2 wHTH domain and eukaryotic C-terminal extension are essential for viability. The indicated Rio2 alleles were tested for complementation of *rio2Δ* (null) by shuffling experiment on SDC plus 5-FOA at 23°C, 30°C and 37°C. +++, complementation at tested temperatures (23, 30, 37°C); -, no complementation (23, 30, 37°C). **(b)** Most of the Rio2 eukaryotic specific C-terminal part is not essential for cell growth in the

presence of *LTV1*$^{+}$. Serial dilutions of the yeast *RIO2* shuffle strain wild-type or deleted for *Ltv1* (see Supplementary Table 2) transformed either with empty plasmid (pRS315), *scRIO2* full-length or different C-terminal deletions were spotted on SDC-Leu (loading control) and SDC plates containing 5-FOA at the indicated temperature for 3 days. **(c)** Overview of the strategy to generate ATP-analogue sensitive protein kinases (see also Supplementary Note). Wild-type kinases contain a conserved "gate-keeper" residue(s) restricting access of bulky ATP-analogs to the ATP-binding pocket (left side). ATP-analogue-sensitive kinases are mutated to enlarge the ATP-binding pocket allowing accommodating of bulky ATP-derivatives (right side). **(d)** Chemical formula of the ATP-analogues CZ14 and 3MB-PP1 used to inhibit *hrr25* I82A and *rio2* V121A M189G kinases, respectively. **(e)** Structural model of *ct*Rio2 V122A M189G (or orthologous *sc*Rio2 V121A M189G). Mutations of residues V122A and M189G were directly introduced into the structure of *ct*Rio2::ATP using the mutagenesis tool of PyMol. Note that the corresponding mutations enlarge the ATP-binding pocket allowing simulated binding of an bulky ATP-analogue. **(f)** *in vivo* inhibition of *rio2* V121A M189G carrying cells in presence of 3MB-PP1. Serial dilutions of yeast strains expressing wild-type *RIO2* or mutants *rio2* were spotted on YPD plates containing either 0.5% DMSO (mock control) or indicated amount of 3MB-PP1 (solved in DMSO) and incubated at the indicated temperatures for 3 days. **(g)** *in vivo* inhibition of *hrr25* I82G carrying cells in presence of CZ14. Serial dilutions of yeast strains expressing wild-type *HRR25* or mutant *hrr25* I89G were spotted on YPD plates containing either 0.25% DMSO (mock control) or indicated amount of CZ14 (solved in DMSO) and incubated at the indicated temperatures for 2 days.

**Supplementary Table 1 | List of strains used in this study.**

| Strain | Genotype | Plasmid | Origin |
|---|---|---|---|
| BY4741/WT | Mat a; his3Δ; leu2Δ; met15Δ; ura3Δ | | Euroscarf |
| rio2Δ /RIO2 diploid | BY4743 Mat a/α; his3Δ/his3Δ; leu2Δ/leu2Δ; LYS2/ lys2Δ; MET15/met15Δ; ura3Δ/ura3Δ; YNL207w/ YNL207w::kanMX4 | | Euroscarf |
| RIO2 shuffle strain | Mat a; his3Δ; leu2Δ; lys2Δ; met15Δ; ura3Δ; YNL207w::kanMX4 | pURA3-RIO2-GFP | this work: derived from rio2Δ/RIO2 diploid |
| RIO2 shuffle strain ltv1Δ | his3Δ; leu2Δ; ura3Δ; YNL207w::kanMX4; YKL143W::kanMX4 | pURA3-RIO2-GFP | this work; offspring from crossing RIO2 shuffle strain with BY4742 ltv1Δ (Euroscarf) |
| RIO2 shuffle strain, Enp1-TAP | Mat a; his3Δ; leu2Δ; lys2Δ; met15Δ; ura3Δ; YNL207w::kanMX4; ENP1-TAP::His3MX6 | pURA3-RIO2-GFP | this work; derived from RIO2 Shuffle strain |
| RIO2 shuffle strain, Ltv1-TAP | Mat a; his3Δ; leu2Δ; lys2Δ; met15Δ; ura3Δ; YNL207w::kanMX4; LTV1-TAP::His3MX6 | pURA3-RIO2-GFP | this work; derived from RIO2 shuffle strain |
| RIO2 shuffle strain, Tsr1-TAP | Mat a; his3Δ; leu2Δ; lys2Δ; met15Δ; ura3Δ; YNL207w::kanMX4; TSR1-TAP::His3MX6 | pURA3-RIO2-GFP | this work; derived from RIO2 shuffle strain |
| HRR25 shuffle strain | his3Δ; leu2Δ; ura3Δ; YPL204w::kanMX4 | pURA3-HRR25 | this work |
| HRR25 shuffle strain, Ltv1-TAP | his3Δ; leu2Δ; ura3Δ; YPL204w::kanMX4; LTV1-TAP::His3MX6 | pURA3-HRR25 | this work |

**Supplementary Table 2 | List of plasmids used in this study.**

| Plasmid | Features | Origin |
|---|---|---|
| pRS315-RIO2 | CEN; LEU2; RIO2 ORF including 500nt before ATG and 140nt after stop codon | this study |
| pRS315-rio2-1 | CEN; LEU2; rio2 mutant ORF including 500nt before ATG and 140nt after stop codon | ref.[4] |
| pRS315-rio2 V121A M189G | CEN; LEU2; rio2 mutant ORF including 500nt before ATG and 140nt after stop codon | this study |
| pRS315-rio2 K123A | CEN; LEU2; rio2 mutant ORF including 500nt before ATG and 140nt after stop codon | this study |
| pRS315-rio2 D229A | CEN; LEU2; rio2 mutant ORF including 500nt before ATG and 140nt after stop codon | this study |
| pRS315-rio2 D253A | CEN; LEU2; rio2 mutant ORF including 500nt before ATG and 140nt after stop codon | this study |
| pRS315-rio2Δ129-146 | CEN; LEU2; rio2 mutant ORF including 500nt before ATG and 140nt after stop codon | this study |
| pRS315-rio2Δ131-146 | CEN; LEU2; rio2 mutant ORF including 500nt before ATG and 140nt after stop codon | this study |
| pRS315-rio2 neutral loop (R129A/ H133A/ R136A/ R139A/ D140A/ K143A/ K144A) | CEN; LEU2; rio2 mutant ORF including 500nt before ATG and 140nt after stop codon | this study |
| pRS315-rio2Δ87-425 | CEN; LEU2; rio2 mutant ORF including 500nt before ATG and 140nt after stop codon | this study |
| pRS315-rio2Δ2-86 | CEN; LEU2; rio2 mutant ORF including 500nt before ATG and 140nt after stop codon | this study |
| pRS315-rio2Δ1-315 | CEN; LEU2; rio2 mutant ORF including 500nt before ATG and 140nt after stop codon | this study |
| pRS315- rio2Δ356-425 | CEN; LEU2; rio2 mutant ORF including 500nt before ATG and 140nt after stop codon | this study |
| pRS315- rio2Δ335-425 | CEN; LEU2; rio2 mutant ORF including 500nt before ATG and 140nt after stop codon | this study |
| pRS315- rio2Δ328-425 | CEN; LEU2; rio2 mutant ORF including 500nt before ATG and 140nt after stop codon | this study |
| pRS315-rio2Δ315-425 | CEN; LEU2; rio2 mutant ORF including 500nt before ATG and 140nt after stop codon | this study |
| pRS315-HRR25 | CEN; LEU2; HRR25 ORF including 880nt before ATG and 865nt after stop codon | this study |
| pRS315-hrr25 I82G | CEN; LEU2; hrr25 I82G ORF including 880nt before ATG and 865nt after stop codon | this study |
| pRS315-RIO2-GFP | CEN; LEU2; RIO2 ORF including 500nt before ATG and 140nt after stop codon | ref. [4] |
| Ycplac111-RIO2-TAP | CEN; LEU2; RIO2 ORF without stop codon fused to the TAP-tag including 500nt before ATG codon | this study |
| Ycplac111-rio2 D253A-TAP | CEN; LEU2; rio2 D253A ORF without stop codon fused to the TAP-tag including 500nt before ATG codon | this study |
| Ycplac111-rio2 neutral loop-TAP | CEN; LEU2; rio2 loop mutant ORF without stop codon fused to the TAP-tag including 500nt before ATG codon | this study |

| | | |
|---|---|---|
| Ycplac111-rio2 K105E-TAP | CEN; LEU2; rio2 loop mutant ORF without stop codon fused to the TAP-tag including 500nt before ATG codon | this study |
| YEP352-GAL::RIO2 | 2μ; URA3; RIO2 ORF under GAL promoter | this study |
| YEP352-GAL::rio2 D253A | 2μ; URA3; RIO2 ORF under GAL promoter | this study |
| YEP352-GAL::rio2 neutral loop | 2μ; URA3; RIO2 ORF under GAL promoter | this study |
| YEP352-GAL::rio2 D253A + neutral loop | 2μ; URA3; RIO2 ORF under GAL promoter | this study |
| Ycplac111-ADH::scRIO2 | CEN; LEU2; ADH promoter; scRIO2 | this study |
| Ycplac111-ADH::*ct*RIO2 | CEN; LEU2; ADH promoter; *ct*RIO2 | this study |
| Ycplac181-ADH::scRIO2 | 2μ; LEU2; ADH promoter; scRIO2 | this study |
| Ycplac181-ADH::*ct*RIO2 | 2μ; LEU2; ADH promoter; *ct*RIO2 | this study |
| pT7::His6-TEV-*ct*RIO2 | E.coli expression vector; Amp | this study |
| pT7::His6-TEV-*ct* rio2 D229A | E.coli expression vector; Amp | this study |
| pT7::His6-TEV-*ct* rio2 D257A | E.coli expression vector; Amp | this study |
| pT7::His6-TEV-*ct* rio2 K106E | E.coli expression vector; Amp | this study |
| pT7::His6-TEV-*ct* rio2 K124A | E.coli expression vector; Amp | this study |
| pT7::His6-TEV-*ct* rio2 „neutral loop“ (R130A/ R134A/ K137A/ R140A/ D141A/ R144A/ R146A) | E.coli expression vector; Amp | this study |

**Supplementary Note: Additional methods**

**Generation of ATP-analogue sensitive yeast strains.** In order to sensitize the Hrr25 and Rio2 kinases to ATP-analogues, a conserved gate-keeper residue mutation, *hrr25* I82G and *rio2* M189G, was introduced as previously described[5]. A series of individual 4-amino-1-*tert*-butyl-pyrazolo[3,4-*d*]pyrimidine derivatives was assayed for growth retardation of *hrr25* I82G and *rio2* M189G using filter assays. The structurally related compounds CZ14, CZ31 and CZ32 were found to be the most potent inhibitor of *hrr25* I82G. Concentration from 1-10 µM of CZ14 effectively inhibited proliferation of *hrr25* I82G mutant cells, but was fully tolerated by the respective wild-type strain. In contrast to *hrr25* I82G cells, only slight cell growth retardation was observed with substances 3MB-PP1, 1NMPP1, 2MeNAPP1, CZ22, and PP1 in the case of the *rio2* M189G mutant. In order to further sensitize the Rio2 kinase we performed a second site mutagenesis (V121A), predicted to enlarge further the ATP-binding pocket. Reduction in cell growth of *rio2* V121A M189G in response to 3MB-PP1 at lower temperature was observed at concentration ranging from 5-25 µM without affecting wild-type cell growth. For further information, see also Supplementary Fig. 5.

**Purification of recombinant *ct*Rio2 and *ct*Hrr25 for single turnover and ATP binding assays.** Recombinant *ct*Rio2 wild-type or mutant proteins were expressed overnight in LB medium containing 100 µg/ml ampicillin and 0.3 mM IPTG at 18°C. *ct*Hrr25 was expressed overnight in M9 minimal medium containing 30 µg/ml kanamycin and 0.3 mM IPTG at 18°C. Cells expressing *ct*Rio2 and *ct*Hrr25 were resuspended in buffer K200 (10% Glycerol, 20 mM Tris-HCl pH 7.5, 200 mM KCl, 10 mM imidazole, 5 mM $MgCl_2$, 2 mM b-mercaptoethanol) and K1500 (same as K200 but with 1.5 M KCl) respectively, and lysed using a microfluidiser. Homogenates clarified by centrifugation at 14,000g for 20 min at 4°C were added to pre-equilibrated Talon-beads (Clontech) (in 0.1% NP-40 and buffer K200 or K1500) and incubated on a rotating wheel for 90 min at 4°C. Beads were washed in batch 4 times 20 min with 20 ml buffer at 4°C, and 3 times 20 ml by gravity flow on a Bio-Rad chromatography column. Proteins were eluted with K200 or K1500 buffer containing 220 mM imidazole. Prior to buffer exchange and concentration the eluted *ct*Hrr25 was incubated overnight at 4°C, and centrifuged for 20 min at 14,000 rpm at 4°C on a bench-top centrifuge. Eluted proteins were buffer

exchanged and concentrated using a Centricon filter (30 kDa cut-off; Millipore) to 50 µM in buffer K200.

**Phosphate release quantification.** To estimate the amount of *ct*Rio2 phosphorylation, a 50 nM ATP/ $g^{32}$P-labeled ATP standard (100% - 0.01%) was spotted on TLC plates, dried and exposed overnight on a Phosphorimager screen. Since the overall amount of g-$^{32}$P-ATP used for *ct*Rio2 auto-phosphorylation was estimated being below 0.1% of the total hydrolysis events, this event was neglected from further quantification.

All quantifications of TLC plates were performed using ImageJ. For every time point the amount of ATP and $P_i$ were determined after subtraction of background. Assuming that most of the hydrolyzed ATP is converted into free phosphate the sum of ATP and Pi radioactivity (in this case phosphorylation of Rio2 is negligible) at different time points represents 100% of the radioactivity loaded on the TLC plate for this time point. Therefore the amount of free phosphate released can be determined for every time points using the following formula:

$$(P_i \text{ in } \%)_{tx} = Pi_{tx}/(ATP_{tx}+Pi_{tx})x100$$

Since for *ct*Hrr25 the amount of ATP is reduced overtime and converted into phosphorylated substrate, the amount of ATP at t=0 was used as normalization constant :

$$(ATP_{t0}=100\%).\ (Pi \text{ in } \%)_{tx} = Pi_{tx}/(ATP_{t0}+Pi_{tx})x100.$$

**ATP-binding experiments.** Reactions (100 µl) were performed in 96 well-plate, were 1 µM of the indicated recombinant proteins was incubated with 0.5 µM of Mant-ATP (Jena bioscience) in buffer K200 for 20 min at 30°C. The mant-ATP was excited at 355 nm with a xenon lamp, and emission spectra were recorded between 385-600 nM with a 5 nm increment step using a Synergy 4 spectrophotometer (BioTek).

**In vitro phosphorylation assay on isolated pre-40S.** Tandem affinity purified pre-40S particles isolated using Ltv1-TAP as a bait were first pre-incubated for 15 min at 23°C in presence of 5µM CZ14 (specific for *hrr25* I82G), 25µM 3MB-PP1 (specific for *rio2* V121A M189G) or in mock-buffer (DMSO). *In vitro* phosphorylation was induced by addition of a mixture of radioactive $\gamma$-$P^{32}$ ATP/ATP (1/1000) for 30 min at 23°C. The $\gamma$-$P^{32}$ labeled pre-40S particles were analyzed by SDS-PAGE/Coomassie staining, followed by

autoradiography of dried gels.

**Miscellaneous.** Polysome profiles and monosomes were analysed by sucrose gradient centrifugation as previously described[6]. Affinity-purifications of TAP-tagged bait proteins were, unless otherwise indicated, performed in a buffer containing 50 mM Tris-HCl, pH 7.5, 100 mM NaCl, 1.5 mM $MgCl_2$, 5% glycerol, and 0.1% NP-40 essentially as described previously[6,7]. For tobacco etch virus (TEV) protease cleavage, DTT and Rnasin (Fermentas) was added to the buffer to a final concentration of 1 mM and 200 U/ml, respectively. Elution from Calmodulin–Sepharose beads was performed for 20 min at 30°C in the presence of 5 mM EGTA. The EGTA eluates were precipitated by the addition of TCA and dissolved in SDS-sample buffer (10-fold concentrated), before separation on NuPAGE SDS 4–12% gradient polyacrylamide gels (Invitrogen) and staining with colloidal Coomassie (Sigma-Aldrich). Mass spectrometry identification of the proteins contained in Coomassie-stained bands was performed as described previously[7]. Western blot analysis was performed using the following primary antibodies: anti-Rio2 (Santa-Cruz, Rio2 Y-220, cat. no. sc-98828; 1:500), anti-ProtA (Sigma, cat. no. P1291; 1:10,000), anti-HA (Covance, cat. no. MMS101R; 1:1,000), anti-rpS3[8](1:5;000), anti-rpS8[8] (1:8,000), anti-Tsr1[2] (1:1,000) and anti-Arc1[9] (1:5,000). Horseradish peroxidase conjugated goat anti-rabbit (Roche, cat. no. 170-6515; 1:8,000) and goat anti-mouse (Bio-Rad, cat. no. 170-6516; 1:3,000) were used as secondary antibodies.

**Supplementary References**


1. Pettersen, E.F. et al. UCSF Chimera--a visualization system for exploratory research and analysis. *J Comput Chem* **25**, 1605-12 (2004).
2. Strunk, B.S. et al. Ribosome assembly factors prevent premature translation initiation by 40S assembly intermediates. *Science* **333**, 1449-53 (2011).
3. Trabuco, L.G., Villa, E., Mitra, K., Frank, J. & Schulten, K. Flexible fitting of atomic structures into electron microscopy maps using molecular dynamics. *Structure* **16**, 673-83 (2008).
4. Schäfer, T., Strauss, D., Petfalski, E., Tollervey, D. & Hurt, E.C. The path from nucleolar 90S to cytoplasmic 40S pre-ribosomes. *EMBO J.* **22**, 1370-1380 (2003).
5. Blethrow, J., Zhang, C., Shokat, K.M. & Weiss, E.L. Design and use of analog-sensitive protein kinases. *Curr Protoc Mol Biol* **Chapter 18**, Unit 18 11 (2004).
6. Kressler, D., Roser, D., Pertschy, B. & Hurt, E. The AAA ATPase Rix7 powers progression of ribosome biogenesis by stripping Nsa1 from pre-60S particles. *J Cell Biol* **181**, 935-44 (2008).
7. Nissan, T.A., Bassler, J., Petfalski, E., Tollervey, D. & Hurt, E. 60S pre-ribosome formation viewed from assembly in the nucleolus until export to the cytoplasm. *EMBO J* **21**, 5539-47 (2002).
8. Schafer, T. et al. Hrr25-dependent phosphorylation state regulates organization of the pre-40S subunit. *Nature* **441**, 651-5 (2006).
9. Simos, G., Sauer, A., Fasiolo, F. & Hurt, E.C. A conserved domain within Arc1p delivers tRNA to aminoacyl-tRNA synthetases. *Mol Cell* **1**, 235-42 (1998).